remote sensing

MDPI

Article

Impact of GPS/BDS Satellite Attitude Quaternions on Precise Point Positioning with Ambiguity Resolution

Songfeng Yang [1], Qiyuan Zhang [1,*], Xi Zhang [2] and Donglie Liu [3]

[1] GNSS Research Center, Wuhan University, Wuhan 430079, China; sfyang@whu.edu.cn
[2] The Third Geodetic Brigade of Ministry of Natural Resources of the People's Republic of China, Chengdu 610199, China; gnss.zhangxi@foxmail.com
[3] Guizhou Provincial First Institute of Surveying and Mapping, Guiyang 550025, China; donglie.liu@westernbeidou.com
* Correspondence: zhangqiyuan@whu.edu.cn

Abstract: Precise point positioning with ambiguity resolution (PPP-AR) based on multiple global navigation satellite system (multi-GNSS) constellations is an important high-precision positioning tool. However, some unmodeled satellite and receiver biases (such as errors in satellite attitude) make it difficult to fix carrier-phase ambiguities. In order to fix ambiguities of eclipsing satellites, accurate integer clock and satellite attitude products (i.e., attitude quaternion) have been provided by the International GNSS Service (IGS). Nevertheless, the quality of these products and their positioning performance in multi-GNSS PPP-AR have not been investigated yet. Using the PRIDE PPP-AR II software associated with the corresponding rapid satellite orbit, integer clock and attitude quaternion products of Wuhan University (WUM), we carried out GPS/BDS PPP-AR using 30 days of data in an eclipsing season of 2020. We found that about 75% of GPS, 60% of BDS-2 and 57% of BDS-3 narrow-lane ambiguity residuals after integer clock corrections fall within ±0.1 cycles in the case of using nominal attitudes. However, when using attitude quaternions, these percentages will rise to 80% for GPS, 70% for BDS-2 and 60% for BDS-3. GPS/BDS daily kinematic PPP-AR after integer clock and nominal attitude corrections can usually achieve a positioning precision of about 10, 10 and 30 mm for the east, north and up components, respectively. In contrast, the counterparts are 8, 8 and 20 mm when using attitude quaternions. Compared with the case of using attitude quaternions only at the network end for the integer clock estimation, using attitude quaternions only at the user end shows a pronounced improvement of 15% in the east component and less than 10% in the north and up components. Therefore, we suggest PPP users apply integer clock and satellite attitude quaternion products to realize more efficient ambiguity fixing, especially in satellite eclipsing seasons.

Keywords: attitude quaternions; satellite eclipsing; precise point positioning; ambiguity resolution; multi-GNSS

Citation: Yang, S.; Zhang, Q.; Zhang, X.; Liu, D. Impact of GPS/BDS Satellite Attitude Quaternions on Precise Point Positioning with Ambiguity Resolution. *Remote Sens.* **2021**, *13*, 3035. https://doi.org/10.3390/rs13153035

Academic Editor: Simon Banville

Received: 7 July 2021
Accepted: 31 July 2021
Published: 2 August 2021

1. Introduction

With the development of precise point positioning (PPP) [1], multi-constellations have become a research hotspot [2–5]. Up to now, global navigation satellite systems (GNSS) such as GPS, GLONASS, Galileo and BDS have provided services worldwide. However, some un-modeled satellite and receiver biases negate the integer property of carrier-phase ambiguities [6] which limits the positioning accuracy and leads to a long convergence time [7]. Fortunately, some methods have been realized to separate the phase biases from undifferenced float ambiguities to recover the integer property of these ambiguities [8–10]. A well-known model is that the fractional-cycle parts of wide-lane ambiguities can be obtained based on the Hatch-Melbourne-Wübbena (HMW) combination [11–13], and then narrow-lane ambiguities can be estimated as integers after narrow-lane phase bias corrections.

In addition, the errors caused by different satellite attitude models impair the accuracy of ambiguity-float PPP solutions [14]. Currently, the nominal attitude for a satellite is generally defined as follows. The *X*-axis is pointing roughly to the sun and perpendicular to the Y/Z plane, with the *Y*-axis along the solar panel and the *Z*-axis towards the earth [15]. However, when most yaw-steering satellites enter the low Sun elevation angle, the nominal attitude model cannot describe the sharp flip at orbit noon/midnight, which causes some errors of satellite attitude, especially when the sun elevation angle is close to 0. Therefore, some satellite manufacturers and academic organizations developed special attitude models during eclipsing periods.

Before 1997, the GPS constellation comprised Block I, Block II and Block IIA satellites. Bar-Sever [16] built the first numerical non-nominal attitude model named as GPS Yaw Model 1994 (GYM94), with yaw bias, shadow crossing maneuver, noon/midnight maneuver and recovery maneuver described quantitatively. Then, the analytical model GYM95 was established to simplify GYM94 [17]. After the first BLOCK IIR satellite was fully operational, Bar-Sever [18] added the non-nominal attitude model for this satellite type/block. In this model, there are no yaw biases or shadow crossing maneuvers, and the yaw rate is larger than that of former GPS satellites. The first Block IIF satellite was launched in 2010, and this satellite type has yaw bias and shadow crossing maneuver, but no extra recovery after exiting the shadow [19,20]. The latest Block IIIA satellites lack an accurate attitude model, and thus Steigenberger et al. [21] alternatively recommended the non-nominal attitude model of Block IIR.

The BDS constellation consists of geosynchronous Earth orbit (GEO), inclined geosynchronous satellite orbit (IGSO) and medium Earth orbit (MEO) satellites from two generations, including BDS-2 and BDS-3. For BDS-2, GEO satellites use orbit-normal mode, so the yaw angle is always zero. IGSO satellites and part of MEO satellites also turn to orbit-normal mode when the sun elevation angle to the orbital plane falls in $[-4^\circ, 4^\circ]$ [22,23]. Besides, even though the satellites SVN C005, C015, C017 and C019 belong to BDS-2, they abandoned orbit-normal mode and adopted the same attitude model as MEO of BDS-3 [24]. BDS-3 satellites are produced by two manufacturers, China Academy of Space Technology (CAST) and Shanghai Engineering Center for Microsatellites (SECM), and these two groups of satellites have different attitude models [25,26]. The yaw behavior of CAST satellites mainly comprised of MEO and IGSO is similar to that of the public released Galileo Full Operation-Capacity (FOC) model. When the sun elevation angle falls into $[-3^\circ, +3^\circ]$ and the orbit angle is -6° or 174°, the yaw maneuver starts. As for MEO satellites of SECM, the yaw angle is calculated using the fixed sun elevation angle (i.e., 3°), if the real sun elevation angle falls in $[-3^\circ, +3^\circ]$.

The Galileo satellite attitude model issued by the European GNSS Agency has been shared among different analysis centers and users [27], while the official attitude documentation of other GNSS, such as GPS and BDS, have not been shared by the system providers. In order to obtain high-precision solutions, an analysis center has to establish a satellite model that describes the true attitude of GPS and BDS. However, different analysis centers may provide inconsistent models, especially those in eclipsing seasons. In addition, since there is no official source code of true attitude model to be released to the public, users usually implement the nominal attitude model. In the processing of PPP model, the errors of satellite yaw attitude can influence the accuracy of phase center variation/offset and phase wind-up, leading to a low-precision positioning performance. Therefore, the consistency of satellite attitude models between network and user ends must be ensured [4]. However, it is not a common strategy that analysis centers provide attitude information for users. Fortunately, in order to solve this problem, exchanging multi-GNSS satellite attitude information in the ORBit EXchange (ORBEX) format is being tested [14,28,29]. Based on this format, Wuhan University (WUM) generated attitude quaternion products, associated with satellite integer clock and orbit products for users [30]. Nevertheless, the quality of these products and their positioning performance in multi-GNSS PPP-AR have not been investigated.

In this paper, we aim at studying the impact of the GPS/BDS attitude quaternions in ORBEX format on PPP-AR, as well as their impact on network and user ends. Note that we estimate satellite clocks based on the integer recovery clock theory [10], and these clocks actually absorb the narrow-lane phase biases and attitude errors. This study is organized as follows: in the following section, we describe the multi-GNSS PPP model. Then, the data processing strategies are shown. After that, we display the impact of different integer clock products based on attitude quaternions or nominal attitudes, and make a GPS/BDS PPP-AR experiment with the PRIDE PPP-AR II software to confirm the positioning performance after using these attitude quaternions. Finally, we draw the conclusions.

2. PPP Model at Network and User Ends

First, we list the basic GNSS observational equations:

$$\begin{cases} P_{j,1}^k = \rho_j^k + c\left(t_j - t^k\right) + I_j^k + b_{j,1} - b_1^k + a_j^k \\ P_{j,2}^k = \rho_j^k + c\left(t_j - t^k\right) + \frac{f_1^2}{f_2^2} I_j^k + b_{j,2} - b_2^k + a_j^k \\ L_{j,1}^k = \rho_j^k + c\left(t_j - t^k\right) - I_j^k + \lambda_1 N_{j,1}^k + B_{j,1} - B_1^k + a_j^k \\ L_{j,2}^k = \rho_j^k + c\left(t_j - t^k\right) - \frac{f_1^2}{f_2^2} I_j^k + \lambda_2 N_{j,2}^k + B_{j,2} - B_2^k + a_j^k \end{cases} \tag{1}$$

$$\rho_j^k = \sqrt{\left(\widetilde{X^k} - X_j\right)^2 + \left(\widetilde{Y^k} - Y_j\right)^2 + \left(\widetilde{Z^k} - Z_j\right)^2} + T_j^k$$

where $P_{j,1}^k$, $P_{j,2}^k$ are pseudorange and $L_{j,1}^k$, $L_{j,2}^k$ are carrier-phase observed values for L1/L2 of GPS and L2/L6 of BDS signals respectively; ρ_j^k is the real geometric distance and it has included the slant troposphere delays T_j^k; $\left(\widetilde{X^k}\ \widetilde{Y^k}\ \widetilde{Z^k}\right)$ and $\left(X_j\ Y_j\ Z_j\right)$ are satellite and receiver coordinates respectively; c is the speed of light; t_j and t^k are the clock errors for receiver and satellite; I_j^k and $\frac{f_1^2}{f_2^2} I_j^k$ are the first-order ionosphere delays and they are related to signal frequencies f_1 and f_2; λ_1 and λ_2 are the wavelengths; $N_{j,1}^k$ and $N_{j,2}^k$ are the integer ambiguities; $b_{j,1}$ and b_1^k are the code hardware delays on signal L1 of GPS and L2 of BDS for receiver j and satellite k, respectively, while $b_{j,2}$ and b_2^k are those on signal L2 of GPS and L6 of BDS; similarly, $B_{j,1}$ and B_1^k are the phase biases on the first frequency, while $B_{j,2}$ and B_2^k are those on the second; a_j^k is the error between the used attitude model and real attitude. Note that the satellite attitude is presented in the form of four quaternions $(q_1\ q_2\ q_3\ q_4)$, and the satellite-body frame unit vectors $\left(\vec{e_x}\ \vec{e_y}\ \vec{e_z}\right)$ are denoted as Equation (2) [14]. The yaw angle is the angle between $\vec{e_x}$ and the orbital along-track direction, and a_j^k is the errors resulted by the inaccurate yaw angle:

$$\begin{aligned} \vec{e_x} &= \begin{bmatrix} q_1^2 + q_2^2 - q_3^2 - q_4^2 \\ 2(q_2 q_3 - q_1 q_4) \\ 2(q_2 q_4 - q_1 q_3) \end{bmatrix} \\ \vec{e_y} &= \begin{bmatrix} 2(q_2 q_3 - q_1 q_4) \\ q_1^2 - q_2^2 + q_3^2 - q_4^2 \\ 2(q_3 q_4 - q_1 q_2) \end{bmatrix} \\ \vec{e_z} &= \begin{bmatrix} 2(q_2 q_4 - q_1 q_3) \\ 2(q_3 q_4 - q_1 q_2) \\ q_1^2 - q_2^2 - q_3^2 + q_4^2 \end{bmatrix} \end{aligned} \tag{2}$$

In order to eliminate the first-order ionosphere delays, the ionosphere-free combination is used [31]:

$$\begin{cases} P_{j,IF}^k = \rho_j^k + c\left(t_j - t^k\right) + b_{j,IF} - b_{IF}^k + a_{j,IF}^k \\ L_{j,IF}^k = \rho_j^k + c\left(t_j - t^k\right) + \alpha\lambda_1 N_{j,1}^k - \beta\lambda_2 N_{j,2}^k + B_{j,IF} - B_{IF}^k + a_{j,IF}^k \end{cases} \tag{3}$$

where $P_{j,IF}^k$ and $L_{j,IF}^k$ are the pseudorange and carrier-phase observations of the ionosphere-free combination; $b_{j,IF}$ and b_{IF}^k are the ionosphere-free code hardware delays at the receiver and satellite; $B_{j,IF}$ and B_{IF}^k are the ionosphere-free phase biases at the receiver and satellite; $a_{j,IF}^k$ is the attitude error of the ionosphere-free combination; the coefficients $\alpha = \frac{f_1^2}{f_1^2 - f_2^2}$ and $\beta = \frac{f_2^2}{f_1^2 - f_2^2}$ are related to the ionosphere-free combination.

In addition, we have the HMW combination observable:

$$L_{j,w}^k = \lambda_w\left(\frac{L_{j,1}^k}{\lambda_1} - \frac{L_{j,2}^k}{\lambda_2}\right) - \frac{f_1 P_{j,1}^k + f_2 P_{j,2}^k}{f_1 + f_2} = \lambda_w\left(N_{j,w}^k + \frac{b_{j,1} - b_1^k}{\lambda_1} - \frac{b_{j,2} - b_2^k}{\lambda_2}\right) - \lambda_n\left(\frac{B_{j,1} - B_1^k}{\lambda_1} - \frac{B_{j,2} - B_2^k}{\lambda_2}\right) \tag{4}$$

where $\lambda_w = \frac{c}{f_1 - f_2}$ and $\lambda_n = \frac{c}{f_1 + f_2}$ are the wavelength of wide-lane and narrow-lane ambiguities, respectively. Wide-lane ambiguities can be calculated with the $L_{j,w}^k$ observable, whereas their receiver and satellite phase biases are:

$$\begin{cases} B_{j,w} = \lambda_w\left(\frac{b_{j,1}}{\lambda_1} - \frac{b_{j,2}}{\lambda_2}\right) - \lambda_n\left(\frac{B_{j,1}}{\lambda_1} - \frac{B_{j,2}}{\lambda_2}\right) \\ B_w^k = \lambda_w\left(\frac{b_1^k}{\lambda_1} - \frac{b_2^k}{\lambda_2}\right) - \lambda_n\left(\frac{B_1^k}{\lambda_1} - \frac{B_2^k}{\lambda_2}\right) \end{cases} \tag{5}$$

The wide-lane phase biases can be estimated with an integer rounding operation after correcting for the phase biases in Equation (5). Note that the attitude errors in Equations (4) and (5) have been eliminated, and thus the wide-lane phase biases are not influenced by the attitude errors.

Once wide-lane ambiguities are resolved, we substitute $N_{j,2}^k = N_{j,1}^k - \overline{N_{j,w}^k}$ into Equation (3) and the ionosphere-free combination can be transformed as:

$$\begin{cases} P_{j,IF}^k = \rho_j^k + c\left(t_j - t^k\right) + b_{j,IF} - b_{IF}^k + a_{j,IF}^k \\ \overline{L_{j,IF}^k} = L_{j,IF}^k - \beta\lambda_2\overline{N_{j,w}^k} = \rho_j^k + c\left(t_j - t^k\right) + \lambda_n N_{j,1}^k + B_{j,IF} - B_{IF}^k + a_{j,IF}^k \end{cases} \tag{6}$$

where $\overline{N_{j,w}^k}$ denotes the resolved wide-lane ambiguity; $\overline{L_{j,IF}^k}$ is the new ionosphere-free carrier-phase data after correction for the resolved wide-lane ambiguity; $N_{j,1}^k$ is also called narrow-lane ambiguity; the wavelength of narrow-lane ambiguities λ_n can be obtained by means of a simple deduction.

In order to obtain the integer recovery clock products, the phase bias and code delay can be transformed as:

$$\begin{cases} B_{IF}^k = B_{IF,0}^k + B_{IF,1}^k \\ b_{IF}^k = b_{IF,0}^k + b_{IF,1}^k \\ B_{j,IF} = B_{j,IF,0} + B_{j,IF,1} \\ b_{j,IF} = b_{j,IF,0} + b_{j,IF,1} \end{cases} \tag{7}$$

where B_{IF}^k can be transformed as the integr portion $B_{IF,0}^k$ and the fractional portion $B_{IF,1}^k$, respectively; $B_{j,IF}$, b_{IF}^k and $b_{j,IF}$ are similar;

Then, Equation (6) can be converted into:

$$\begin{cases} P_{j,IF}^k = \rho_j^k + c\left(t_j + \frac{b_{j,IF,0}+B_{j,IF,1}}{c}\right) - c\left(t^k + \frac{b_{IF,0}^k+B_{IF,1}^k}{c} - \frac{a_{j,IF}^k}{c}\right) + b_{j,IF,1} - b_{IF,1}^k - B_{j,IF,1} + B_{IF,1}^k \\ \overline{L_{j,IF}^k} - \lambda_n \overline{N_{j,1}^k} = \rho_j^k + c\left(t_j + \frac{b_{j,IF,0}+B_{j,IF,1}}{c}\right) - c\left(t^k + \frac{b_{IF,0}^k+B_{IF,1}^k}{c} - \frac{a_{j,IF}^k}{c}\right) \end{cases} \quad (8)$$

where $\overline{N_{j,1}^k}$ is the resolved narrow-lane ambiguity which has been fixed to integers, and $\overline{N_{j,1}^k}$ has actually absorbed the integr portions of the phase bias and code delay; $c\left(t^k + \frac{b_{IF,0}^k+B_{IF,1}^k}{c} - \frac{a_{j,IF}^k}{c}\right)$ is the integer clock and the phase bias (i.e., $b_{IF,0}^k + B_{IF,1}^k$) as well as the attitude error (i.e., $a_{j,IF}^k$) are absorbed by this parameter; $c\left(t_j + \frac{b_{j,IF,0}+B_{j,IF,1}}{c}\right)$ is the receiver clock error; the nuisance term $b_{j,IF,1} - b_{IF,1}^k - B_{j,IF,1} + B_{IF,1}^k$ will be eventually driven into the pseudorange residuals. This term includes the minor fractional portions of the phase bias and code delay. Moreover, we note that the errors between the used attitude model and real attitude can be partly absorbed into the integer clock.

After obtaining the wide-lane phase bias and integer clock products, the user end can use these products to correct ionosphere-free combination observable to realize PPP-AR, that is

$$\begin{cases} P_{j,IF}^k + c\widetilde{t^k} \approx \rho_j^k + c\hat{t}_r \\ L_{j,IF}^k + \widetilde{B_w^k} = \lambda_w N_{j,w}^k + B_{j,w} \\ L_{j,IF}^k + c\widetilde{t^k} - \beta\lambda_2 \overline{N_{j,w}^k} = \rho_j^k + c\hat{t}_r + \lambda_n N_{j,1}^k \end{cases} \quad (9)$$

where $\widetilde{t^k}$ is the integer satellite clock product; $\hat{t}_r$ is the receiver clock estimated; $\widetilde{B_w^k}$ is the wide-lane phase bias product. Using $\widetilde{B_w^k}$, the wide-lane ambiguities with integer nature (i.e., $\overline{N_{j,w}^k}$) are obtained. Note that the term $b_{j,IF,1} - b_{IF,1}^k - B_{j,IF,1} + B_{IF,1}^k$ presented in Equation (8) is disregarded here since it cannot be estimated explicitly (note the symbol "≈" in Equation (9)).

3. Data Processing

In order to show the impact of attitude quaternion/nominal attitude models on the generation of integer clock products (the network end) and PPP-AR (the user end), we implemented some GPS/BDS PPP-AR experiments using PRIDE PPP-AR II software. As shown in Figure 1, we picked 184 evenly distributed International GNSS Service (IGS) stations [32] to compute satellite integer clocks, and 490 globally distributed IGS stations to conduct PPP-AR. We collected 30 s data from day 081 to 110 of 2020. The data processing strategies are listed in Table 1. In the kinematic experiments, ambiguity fixing was achieved through the bootstrapping bias fixing method [33]. The sequential bias fixing strategy was applied with a round-off criteria of 0.20 cycles for wide-lane ambiguities and 0.15 cycles for narrow-lane ambiguities. Besides, the mean short observation arcs that do not exceed an elevation of 15°, or less than 600 s were not fixed. At each station, the epochs with less than four satellites were removed. A threshold of five times the standard deviation of daily kinematic station coordinates was used to remove those outlier epochs. Then the position accuracy was defined as the mean values of standard deviations. Note that the GEO satellites of BDS were excluded because of their low-precision orbits.

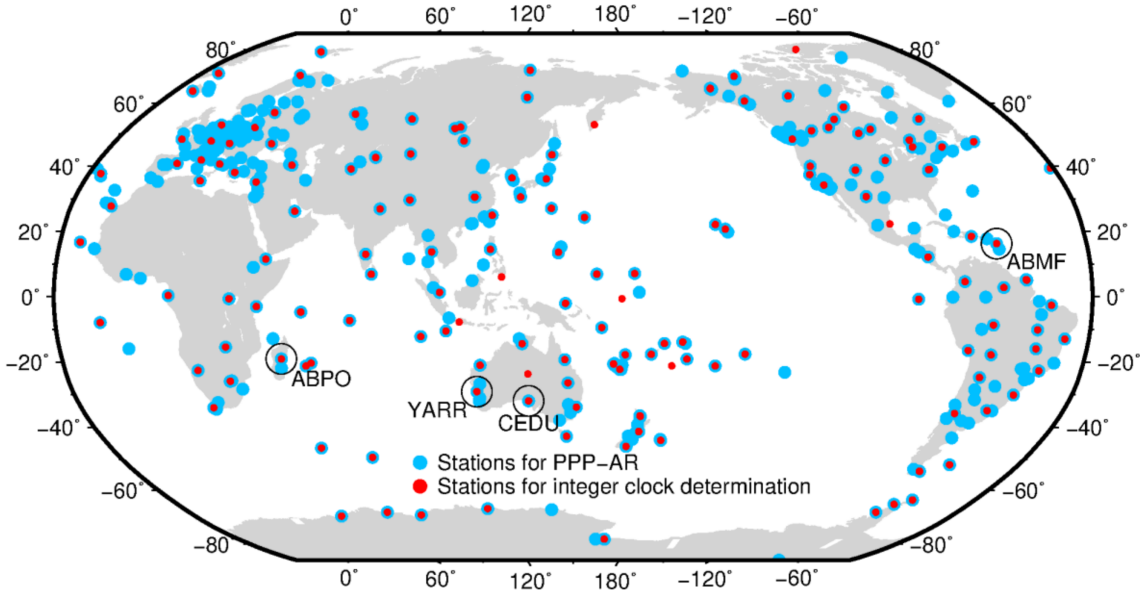

Figure 1. Distribution of used IGS stations. 184 stations (red dots) are used for integer clock products computation and 490 stations (blue dots) are used for PPP-AR experiments.

Table 1. Processing strategies of PPP-AR.

Items	Strategies
Observables	Ionosphere-free combination
Cut-off elevation	7°
Sampling rate	30 s
Weighting	Elevation-dependent for satellites;Equally weighted for GNSS
Solid Earth tide, ocean tidal loading, pole tide	IERS conventions 2010 [34]
Nadir-dependent pseudorange biases of BDS-2	Corrected [35]
Phase center offsets/variations	igs14.atx
Phase wind-up	Corrected [36]
Satellite attitude	Nominal attitude: Corrected by nominal attitude modelAttitude quaternions: WUM rapid products
Earth rotation parameters	WUM rapid products
Precise satellite orbits	WUM rapid products
Precise satellite clocks	WUM rapid products
Position coordinates	estimated as white-noise like parameter at each epoch
Receiver clocks	estimated as white-noise like parameter per epoch for each GNSS system
Zenith tropospheric delays	Piece-wise constants per hour
Horizontal tropospheric gradients	Piece-wise constants per 12 h
Ambiguities	Real-valued constants for each continuous arc

In our simulated daily kinematic experiments, as listed in Table 2, we designed four strategies to conduct PPP-AR to investigate the impact of attitude quaternions on integer clock products and ambiguity fixing. Strategy (a) generated integer clocks by using nominal attitude at the network end, and carried out PPP-AR by using nominal attitude at the user end; strategy (b) only used attitude quaternions at the network end, and still used nominal attitude at the user end; In contrast, strategy (c) only used attitude quaternions at the user end; strategy (d) used attitude quaternions at both network and user ends.

Table 2. Attitude quaternions using strategies to investigate the impact on integer clock products.

	Network End	User End
Strategy (a)	Using nominal attitude	Using nominal attitude
Strategy (b)	Using attitude quaternions	Using nominal attitude
Strategy (c)	Using nominal attitude	Using attitude quaternions
Strategy (d)	Using attitude quaternions	Using attitude quaternions

4. Impact on Integer Clock Products

At the network end, the integer clock products generated with the nominal attitude or attitude quaternions during the eclipsing periods are different, and these integer clock products can influence the efficiency of ambiguity fixing. Therefore, it is essential to validate the quality of integer clock products generated with the nominal attitude or attitude quaternions. Note that the fundamental idea behind the integer clock model is that the narrow-lane phase biases are absorbed into satellite clocks, thereby we actually analyzed the impact on clock products.

In order to analyze the different impact on integer clock products of different types of satellites, we made the comparisons of GPS and BDS integer clocks. The wide-lane phase biases were all calculated only using raw GNSS data, so they keep consistent with different attitude correction models. The narrow-lane phase biases are actually absorbed into the satellite clocks, so we show the time series of double-difference satellite clocks of GPS and BDS (see Figure 2). First, we selected satellite G01 and C06 as references to form the single-difference satellite clocks to remove the changes of benchmarks. Second, we shaped the double-difference satellite clocks (see red dots) between those estimated by the nominal attitude and attitude quaternions, respectively. The gray zones denote the satellite eclipsing periods. A total of eight eclipsing satellites (G08, G12, G27, G32, C14, C16, C30 and C34) are plotted to show the different impact on integer clock products. The sun elevation angles of these satellites are also shown in the figure. Clearly, GPS and BDS integer clocks with different attitude models all show differences. The maximum differences occur in C30 and C34 eclipsing periods on day 110, 2020, with root mean square (RMS) errors of higher than 150 ps. In particular, even though we plot the gray eclipsing zones of C30 and C34 panels, the large attitude errors between the nominal attitude and attitude quaternion models almost exist all day because these satellites maintain the 3-degree sun elevation on this day. Compared with eclipsing satellites G08, G27 and G32, G12 shows the shorter eclipsing periods, which may cause the smaller RMS errors of double-difference satellite clocks of lower than 20 ps. In addition, we find that the attitude differences of satellites during the eclipsing periods can also influence the integer clocks during the non-eclipsing periods and non-eclipsing satellites (not shown here though). These phenomena reveal that using different attitude corrections influences the common parameters such as ambiguities. An ambiguity parameter almost spans eclipsing and non-eclipsing periods and is estimated as a constant, so this parameter can influence the integer clocks in the non-eclipsing periods. In general, the attitude quaternion products of BDS satellites show a more remarkable impact on integer clock products than those of GPS satellites.

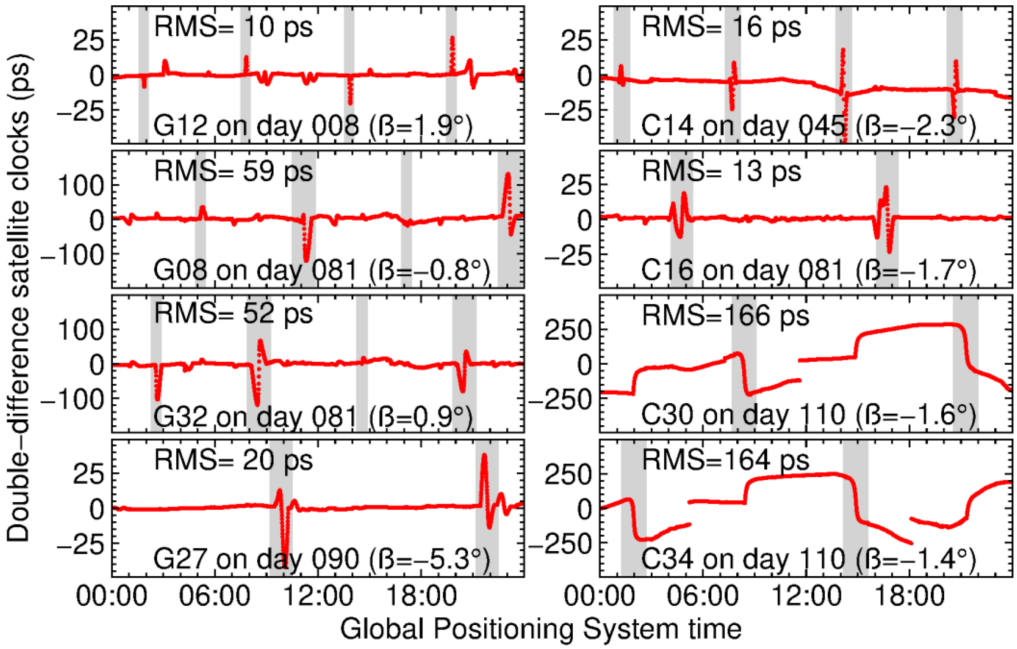

Figure 2. Time series of double-difference satellite clocks for satellites G08, G12, G27, G32, C14, C16, C30 and C34 in 2020. The reference satellites are G01 and C06 for GPS and BDS satellites, respectively. The red dots are the double-difference satellite clocks computed using the clocks based on nominal attitudes and attitude quaternions. The gray zones denote the eclipsing periods of corresponding satellites. The RMS error at the top part of a panel is for the eclipsing period. The average sun elevation angle for corresponding day is shown at the bottom part of a panel. Note that the different panels of the figure have different scales.

In order to recover the integer nature of ambiguities, the integer clock products were used to correct float ambiguities. Thus, we analyzed the residuals of float ambiguities after using integer clock corrections. The float ambiguities were calculated using daily kinematic ambiguity-float PPP from day 081 to 110 of 2020. In this period, there are 6 days for BDS-2, 10 days for BDS-3 and 24 days for GPS to have eclipsing satellites, respectively. As shown in Figure 3, we calculated the residuals of float ambiguities after correcting integer clocks including the provided attitude quaternions at the user end (see blue bars); for another, we also obtained the residuals using the integer clocks including the nominal attitude (see red open bars). After GPS integer clock corrections with the attitude quaternions, about 80% of narrow-lane ambiguity residuals fall within ± 0.1 cycles and its standard deviation is 0.1 cycles, presenting a 4% improvement in residual distribution and a reduction of 0.02 cycles in terms of standard deviation, respectively. Similarly, in the case of BDS-2, the narrow-lane ambiguity residuals have a standard deviation of 0.13 cycles and more than 70% of residuals are within ± 0.1 cycles. The distribution of BDS-2 narrow-lane ambiguity residuals generated with the attitude quaternions shows the most evident improvement. Particularly, BDS-3 doesn't show the huge improvement like BDS-2 though it has longer eclipsing periods. Overall, we demonstrate that the integer clock products generated with attitude quaternions have better performance in recovering integer PPP ambiguities.

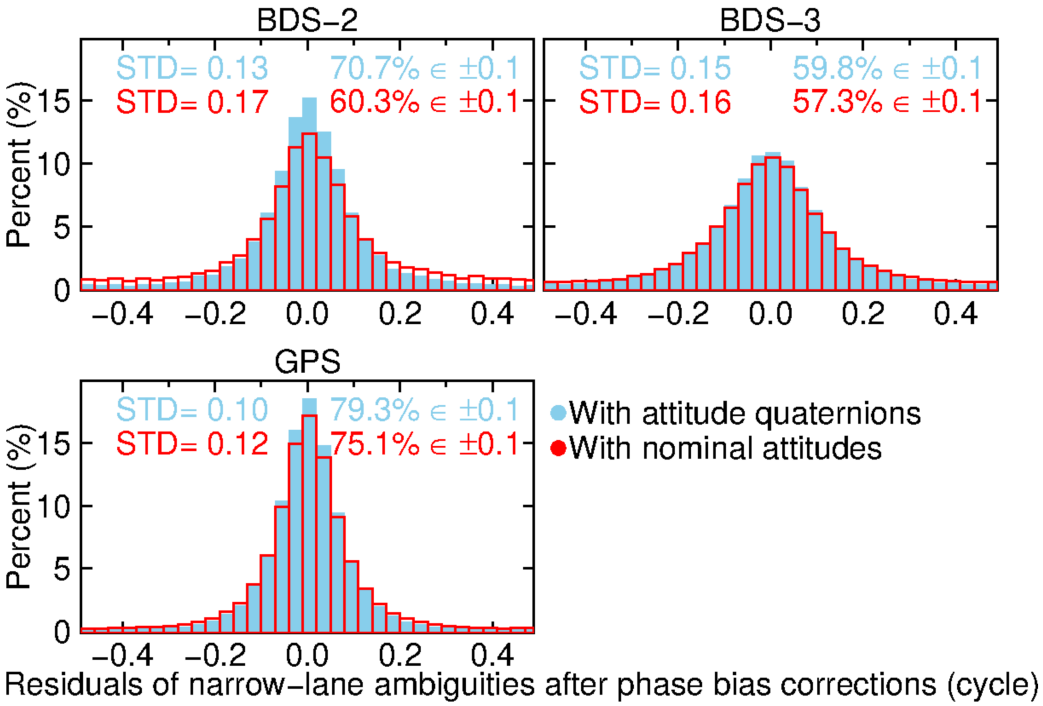

Figure 3. Distribution of GPS, BDS-2 and BDS-3 narrow-lane ambiguity residuals after correcting integer clock products from days 081 to 110 of 2020. The standard deviations of all residuals and the percentages of all within ±0.1 cycles are plotted at the top left and top right corners of each panel, respectively. The blue bar graphs are residuals after correcting integer clock products including the influence of the attitude quaternions; while the red bar graphs are those without the influence of the attitude quaternions or with the influence of nominal attitude.

5. Daily Kinematic Solutions of PPP-AR

At the network end, the integer clock products with attitude quaternions show better performance compared with those with nominal attitude. Meanwhile attitude quaternions were also provided at the user end. In order to show the performance of attitude quaternions in positioning, we carried out kinematic PPP-AR experiments of four strategies as listed in Table 2 using daily data.

Figure 4 shows the two-hour carrier-phase and pseudorange residuals for different types of satellites using the four strategies. The gray zones denote the satellite eclipsing periods. First, the satellite G08 (BLOCK IIF) of station ABPO (shown in Figure 1) on day 082, 2020 and the satellite G19 (BLOCK IIR) of station ABMF on day 089, 2020 were set as an example to compare the residuals. The two GPS satellites are close to deep eclipse during these two periods. As shown in the top panel of Figure 4, the carrier-phase residuals of G08 for strategies (a), (b) and (c) all fluctuate significantly in the case of using nominal attitude, or inconsistent attitude. Their RMSs in the eclipsing periods are higher than 0.05 cycles. In contrast, once the attitude quaternions are applied at network and user ends, the carrier-phase residuals flatten out, with RMS of 0.03 cycles. Note that carrier-phase residuals of G19 also show clear differences in the eclipsing period, even though the eclipsing period is shorter than five minutes. Second, for representative BDS-2 satellites C06 (IGSO) and C14 (MEO) shown in the bottom panel of Figure 4, respectively, observed by station CEDU on day 086 for the former and station YARR on day 050 for the latter in 2020, the carrier-phase residuals also represent different performance. For the eclipsing period spanning eclipsed satellite C06, the RMSs of residuals are decreased from 0.05 to 0.02 cycles after using the attitude quaternions at user ends, equating a 60% improvement. We can see a near-constant offset in carrier-phase residuals for C06 beginning at the center of the shadow crossing when using strategies (c) and (d) compared to (a) and (b). This is resulted

by the minor errors when using attitude quaternions only at the user end, and these errors make fixed ambiguities inaccurate in ambiguity arcs. Since ambiguity estimates can extend from the eclipsing to the non-eclipsing periods, the difference of residuals will still exist in non-eclipsing periods. In contrast, C14 has the fundamentally similar residuals for all strategies, and their RMSs are about 0.04 cycles. Moreover, the pseudorange residuals are much smaller than their noise level, as evidenced by the quasi-overlaps of dots from four strategies.

As shown in Figure 5, four strategies of the usage of attitude correction models indicate the different narrow-lane fixing rates. Strategy (d) achieves the highest fixing rates of all, about 90, 79 and 77% for GPS, BDS-2 and BDS-3, respectively. Generally, this strategy can lead to an improvement of about 10% for BDS-2 while GPS and BDS-3 satellites show modest improvements of less than 5% compared to other strategies. It shows that the attitude quaternions we used are helpful to improve the performance of fixing ambiguities, especially for BDS-2. In contrast, the narrow-lane fixing rates of strategy (b) are 85, 71 and 72%. This worst performance of fixing rates is mainly caused by attitude quaternions being only used at the network end to generate integer clocks, but not introduced at the user end, which leads to inconsistencies. With the nominal attitude corrections at both network and user ends, strategy (a) shows higher fixing rates than (b) and (c) except for BDS-2. However, strategy (c) achieves higher narrow-lane fixing rates within them, about 87, 72 and 75%. This phenomenon demonstrates the biases caused by the inaccurate attitude model cannot be absorbed into integer clock products entirely. The satellite clocks and orbits are also affected by the inaccurate attitude at the network end.

Table 3 shows the mean standard deviations of ambiguity-float and ambiguity-fixed solutions over all stations for the 30 days, as well as the improvements after fixing ambiguities. In fact, all strategies can lead to a pronounced positioning improvement of over 20% in the east component while the north and up components show modest improvements of less than 12%, as exhibited by the last column of Table 3. Moreover, strategy (b) shows the lowest position accuracy independent of float or fixed solutions compared to other strategies.

In order to investigate the daily positioning performance of ambiguity-fixed PPP based on strategies (a), (b), (c) and (d), we plot the standard deviations of GPS/BDS ambiguity-fixed solutions in the east, north and up components at 490 stations. As shown in Figures 6–8, when a dot is located above the black diagonal line, the standard deviation of position errors corresponding to the strategy on the horizontal axis is smaller than that corresponding to the strategy on the vertical axis. It is clear that using attitude quaternions at both network and user ends can improve the position accuracy for kinematic solutions (see panels IV, V and VI), realizing the mean standard deviations of 7.8, 8.4 and 23.2 mm in the east, north and up components, thus echoing the statistics in Figure 5. In addition, note that strategy (a) has clearly more stations with position standard deviations of over 5, 5 and 15 mm compared with the left two strategies (b) and (c), even though it does not use attitude quaternions at both network and user ends (see panels I, II and IV). Generally, in order to gain the best position solutions, users should apply attitude models or data that are consistent with those used on the network end.

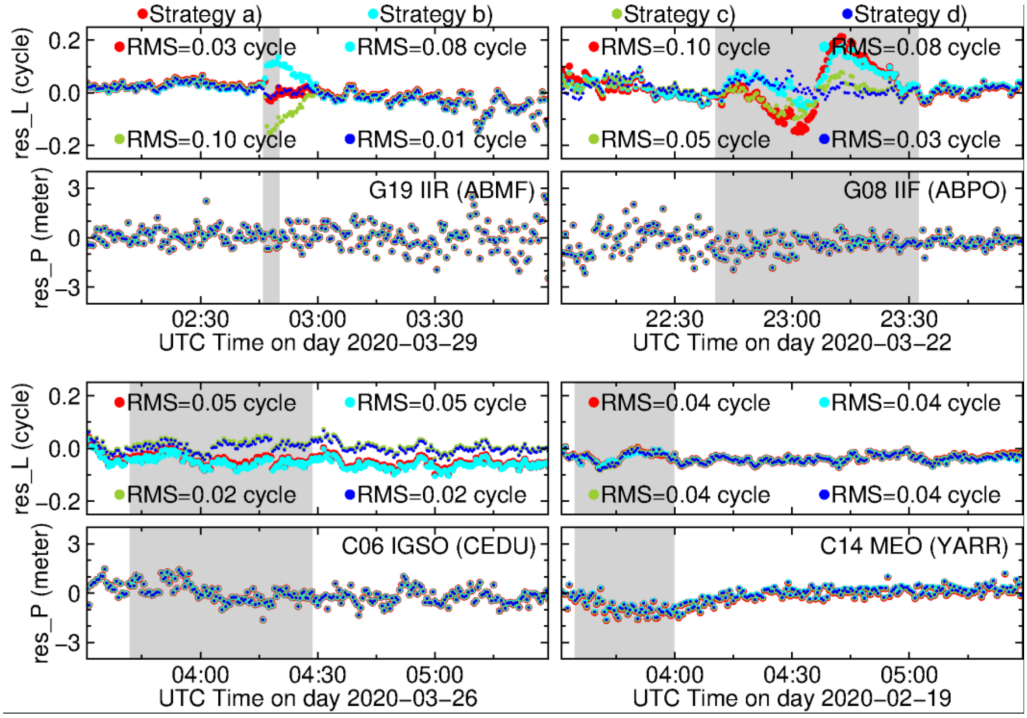

Figure 4. Carrier-phase and pseudorange residuals for different satellite types. Red, cyan, green and blue dots denote the residuals based on strategies (a), (b), (c) and (d), respectively. The gray zones denote the eclipsing periods of corresponding satellites.

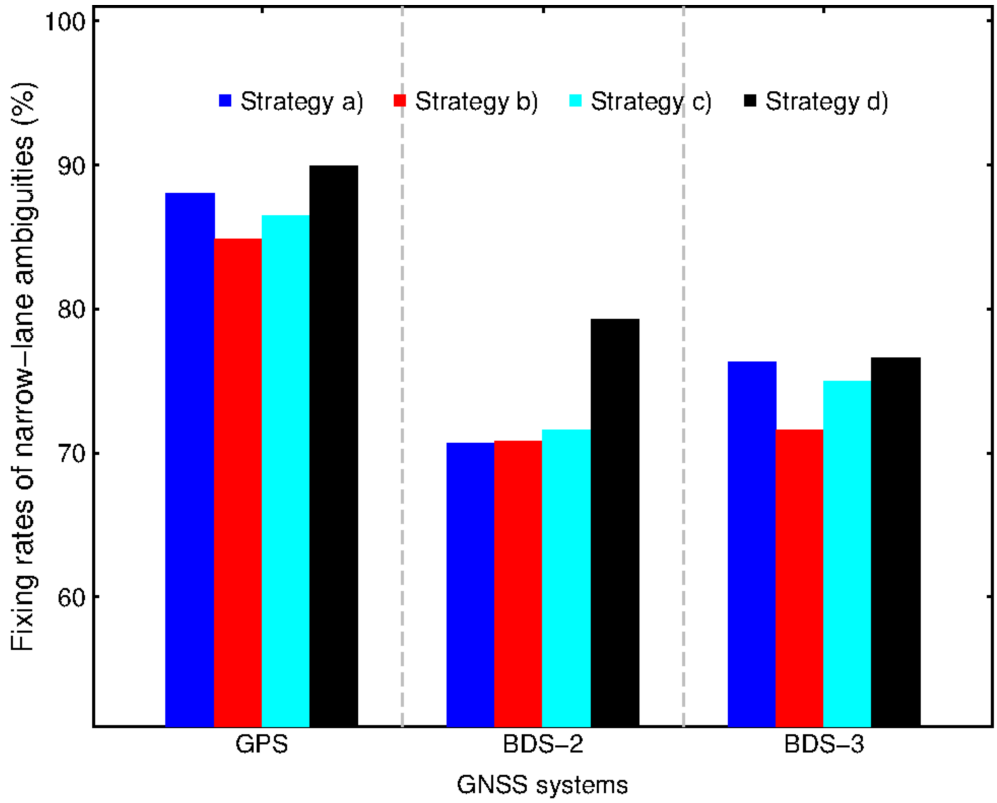

Figure 5. Narrow-lane ambiguity fixing rates (%) for daily kinematic solutions corresponding to four strategies on day 081 to 110, 2020.

Table 3. Mean standard deviations (mm) of position errors for kinematic solutions on day 081 to 110, 2020.

Strategy Names	Float Solutions in Different Directions (mm)	Fixed (mm)	Improvement (%)
	E/N/U	E/N/U	E/N/U
Strategy (a)	11.0/9.7/25.9	8.2/8.7/24.1	25.5/10.3/6.9
Strategy (b)	13.4/11.1/29.4	10.5/10.0/28.0	21.6/9.9/4.8
Strategy (c)	12.2/10.2/27.3	9.0/9.0/25.5	26.2/11.8/6.6
Strategy (d)	10.3/9.3/24.6	7.8/8.4/23.2	24.3/9.7/5.7

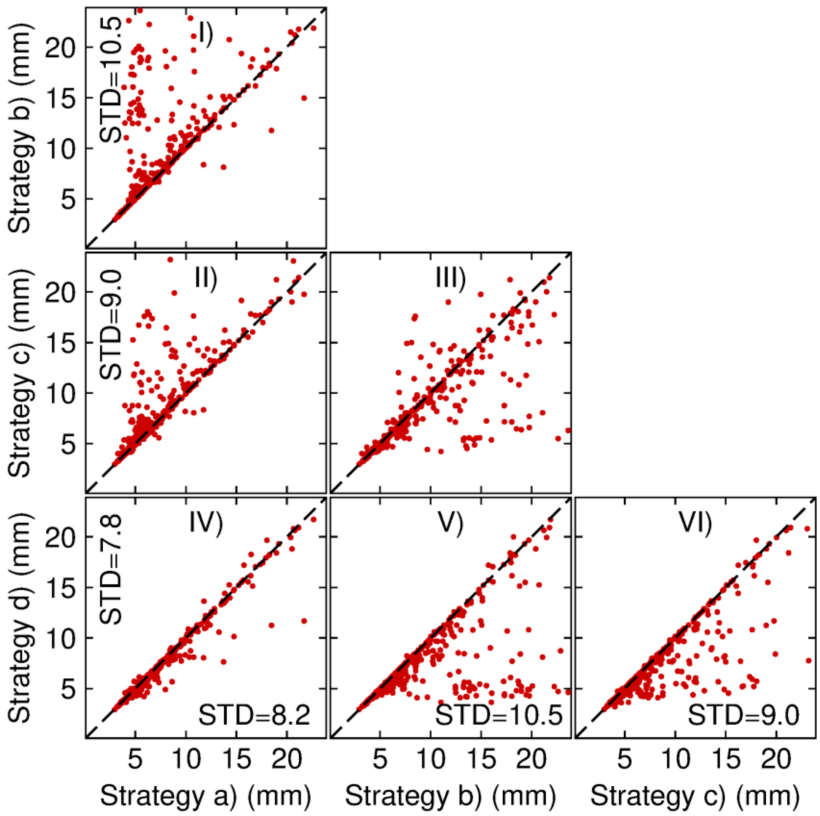

Figure 6. Ambiguity-fixed mean standard deviations of position errors comparison in the east direction between the daily kinematic PPP-AR solutions based on strategies (a), (b), (c) and (d). For I-VI panels, each panel denotes the comparison of two strategies. Each red dot denotes a station. The standard deviations along the horizontal and vertical axes are the mean values of all stations.

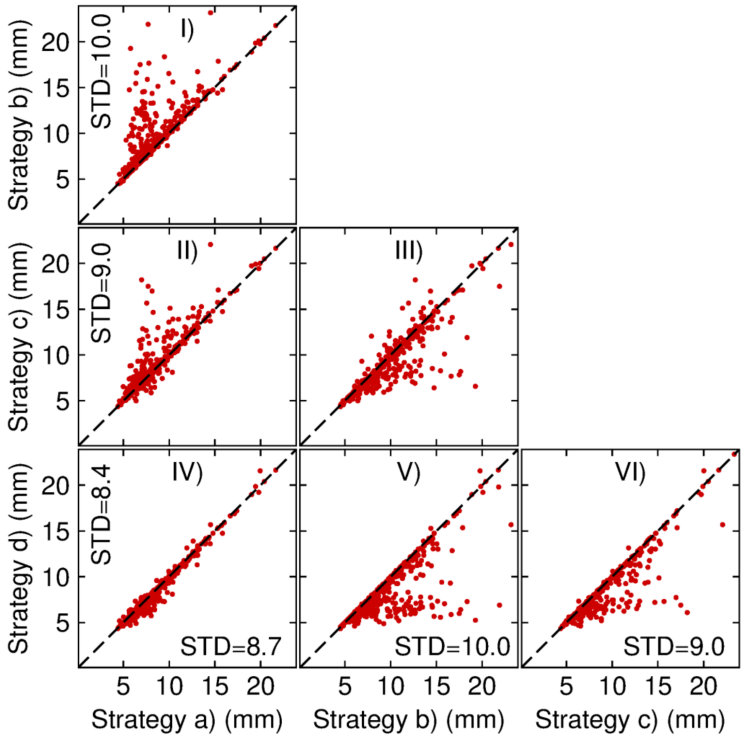

Figure 7. Ambiguity-fixed mean standard deviations of position errors comparison in the north direction between the daily kinematic PPP-AR solutions based on strategies (a), (b), (c) and (d). For I-VI panels, each panel denotes the comparison of two strategies.

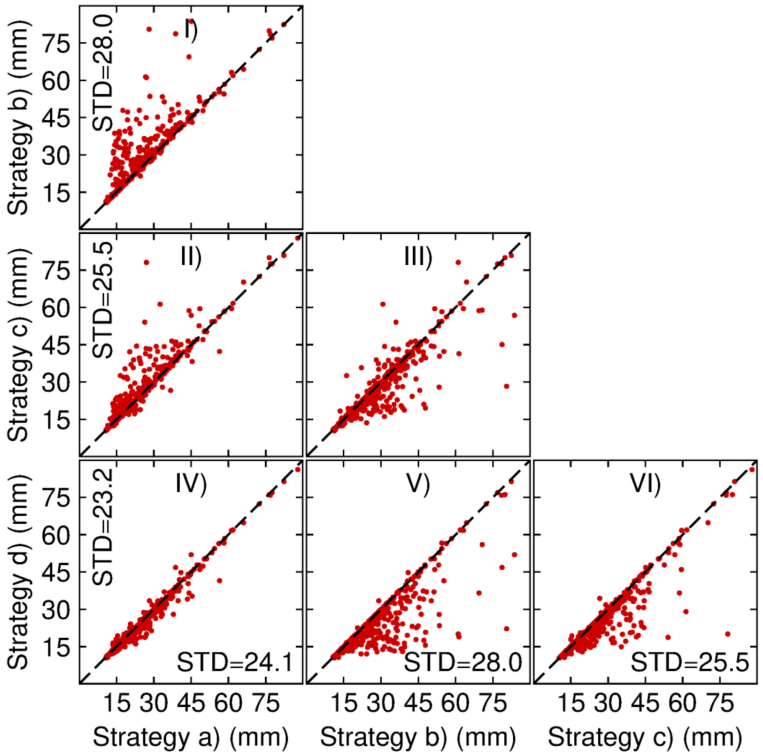

Figure 8. Ambiguity-fixed mean standard deviations of position errors comparison in the up direction between the daily kinematic PPP-AR solutions based on strategies (a), (b), (c) and (d). For I-VI panels, each panel denotes the comparison of two strategies.

6. Discussion

In Figure 3, the integer clock products generated with attitude quaternions have better performance than those generated with nominal attitude in recovering integer PPP ambiguities, while the residuals of float ambiguities after using integer clock corrections for BDS represent more improvements than those for GPS. In this section, we discuss the possible reasons why BDS is more affected by attitude errors.

First, the attitude errors caused by inconsistent satellite attitude models can impact satellite phase center offset corrections. Cleary, BDS satellite C06 have larger phase center offset values, with 580.00, 0.00 and 3500.00 mm in the east, north and up directions on day 086, 2020. In contrast, the phase center offset values for eclipsing satellite G08 are 394.00, 0.00 and 1501.40 mm on this day (see igs14_2136.atx). Therefore, attitude errors of C06 show more impact from mismodelled satellite phase center offset corrections.

Second, parts of BDS-2 satellites adopt orbit-normal mode when the sun elevation to the orbital plane becomes lower than 4°. The nominal attitude model cannot describe precisely the real BDS-2 attitude in eclipsing periods and the attitude errors between the nominal and real attitude are larger than those of GPS.

Third, for BDS-3 satellites produced by SECM, once the real sun elevation angle falls into [−3°, +3°], the yaw angle of this type of satellites will be calculated using the fixed sun elevation angle (i.e., 3°), such as C30 on day 110. In addition, GPS was designed to have six orbital planes, in contrast to three orbital planes for BDS MEO/IGSO. Since BDS has more satellites per orbital plane and the eclipse period depends on the angle of the sun relative to the orbital plane, more BDS satellites will be in eclipse at the same time compared to GPS, where it is more spread out. Therefore, during these periods, the effect of attitude errors is larger for BDS.

7. Conclusions

With the open-source software PRIDE PPP-AR II issued by PRIDE Lab at GNSS Research Center of Wuhan University, the attitude quaternion files in the ORBEX format are also provided to users. In this paper, we compare the integer clock products generated with the nominal attitude and the attitude quaternions, respectively. It shows that different attitude models surely influence the integer clocks which have absorbed narrow-lane phase biases, and the difference is up to 166 ps. Moreover, the eclipsing satellites influence not only the integer clocks during the eclipsing periods, but also those during the non-eclipsing periods. In the case of validating ambiguity residuals after correcting integer clocks generated with the attitude quaternions, about 80% for GPS, 70% for BDS-2 and 60% for BDS-3 ambiguity residuals after integer clock corrections fall within ± 0.1 cycles. However, these percentages fall by 4% for GPS, 10% for BDS-2 and 3% for BDS-3, respectively when using the nominal attitude. This result demonstrates that these GPS/BDS integer clocks can enable kinematic PPP-AR in an efficient manner.

For the GPS/BDS kinematic daily solutions after fixing ambiguities at 490 globally distributed stations with month-long data, using the attitude quaternions at both network and user ends can surely improve the fixing efficiency and position accuracy, and realize the lowest standard deviations of 8 and 20 mm in the horizontal and vertical directions, respectively. Besides, the positioning performance of the experiment using the nominal attitude at both network and user ends is better than that using the attitude quaternions only at network or user ends, which indicates the importance of the consistency between integer clocks and attitude models. In particular, integer clocks cannot absorb all biases caused by different attitude models, thereby it is best that the users apply both the integer clock products and corresponding attitude quaternion products to implement PPP-AR.

Finally, we discuss the reasons why BDS is more affected by attitude errors in our month-long test. Compared with GPS, BDS has larger phase center offset values, and more eclipsing satellites at the same time. In addition, the inaccuracy of a nominal attitude model increases when BDS-2 satellites enter orbit-normal mode. These amplify the errors caused by inconsistent attitude models and make BDS be more affected by attitude errors.

Author Contributions: Conceptualization: S.Y.; Software: S.Y.; Data analysis: S.Y.; Writing: S.Y. and Q.Z.; Editing: S.Y., Q.Z., X.Z. and D.L. All authors read and approved the final manuscript.

Funding: This research was funded by National Science Foundation of China, grant number 42025401.

Institutional Review Board Statement: Not applicable.

Informed Consent Statement: Not applicable.

Data Availability Statement: PRIDE PPP-AR II is an open-source software package which can be downloaded at https://pride.whu.edu.cn (accessed on 24 June 2021).

Acknowledgments: We thank the IGS for the multi-GNSS data and the high-precision satellite products.

Conflicts of Interest: The authors declare no conflict of interest.

References

1. Zumberge, J.F.; Heflin, M.B.; Jefferson, D.C.; Watkins, M.M.; Webb, F.H. Precise point positioning for the efficient and robust analysis of GPS data from large networks. *J. Geophys. Res. Solid Earth* **1997**, *102*, 5005–5017. [CrossRef]
2. Bisnath, S.; Gao, Y. Current state of precise point positioning and future prospects and limitations. In *Observing Our Changing Earth*; Springer: Berlin/Heidelberg, Germany, 2009; pp. 615–623.
3. Cai, C.; Gao, Y.; Pan, L.; Zhu, J. Precise point positioning with quad-constellations: GPS, BeiDou, GLONASS and Galileo. *Adv. Space Res.* **2015**, *56*, 133–143. [CrossRef]
4. Liu, T.; Chen, H.; Chen, Q.; Jiang, W.; Laurichesse, D.; An, X.; Geng, T. Characteristics of phase bias from CNES and its application in multi-frequency and multi-GNSS precise point positioning with ambiguity resolution. *GPS Solut.* **2021**, *25*, 58. [CrossRef]
5. Guo, F.; Li, X.; Zhang, X.; Wang, J. The contribution of Multi-GNSS Experiment (MGEX) to precise point positioning. *Adv. Space Res.* **2017**, *59*, 2714–2725. [CrossRef]
6. Gabor, M.J.; Nerem, R.S. GPS carrier phase ambiguity resolution using satellite-satellite single differences. In Proceedings of the 12th International Technical Meeting of the Satellite Division of the Institute of Navigation (ION GPS 1999), Nashville, TN, USA, 14–17 September 1999; pp. 1569–1578.
7. Geng, J.; Teferle, F.N.; Shi, C.; Meng, X.; Dodson, A.H.; Liu, J. Ambiguity resolution in precise point positioning with hourly data. *GPS Solut.* **2009**, *13*, 263–270. [CrossRef]
8. Ge, M.; Gendt, G.; Rothacher, M.; Shi, C.; Liu, J. Resolution of GPS carrier-phase ambiguities in Precise Point Positioning (PPP) with daily observations. *J. Geod.* **2008**, *82*, 389–399. [CrossRef]
9. Collins, P.; Bisnath, S.; Lahaye, F.; Héroux, P. Undifferenced GPS ambiguity resolution using the decoupled clock model and ambiguity datum fixing. *Navigation* **2010**, *57*, 123–135. [CrossRef]
10. Laurichesse, D.; Mercier, F.; Berthias, J.P.; Broca, P.; Cerri, L. Integer ambiguity resolution on undifferenced GPS phase measurements and its application to PPP and satellite precise orbit determination. *Navigation* **2009**, *56*, 135–149. [CrossRef]
11. Hatch, R. The synergism of GPS code and carrier measurements. In Proceedings of the Third Geodetic Symposium on Satellite Doppler Positioning, Las Cruces, NM, USA, 8–12 February 1982; pp. 1213–1231.
12. Melbourne, W.G. The case for ranging in GPS based geodetic systems. In Proceedings of the 1st International Symposium on Precise Positioning with the Global Positioning System, Rockville, MD, USA, 15–19 April 1985; pp. 373–386.
13. Wübbena, G. Software developments for geodetic positioning with GPS using TI 4100 code and carrier measurements. In Proceedings of the 1st International Symposium on Precise Positioning with the Global Positioning System, Rockville, MD, USA, 15–19 April 1985; pp. 403–412.
14. Loyer, S.; Banville, S.; Geng, J.; Strasser, S. Exchanging satellite attitude quaternions for improved GNSS data processing consistency. *Adv. Space Res.* **2021**, *68*, 2441–2452. [CrossRef]
15. Montenbruck, O.; Schmid, R.; Mercier, F.; Steigenberger, P.; Noll, C.; Fatkulin, R.; Kogure, S.; Ganeshan, A.S. GNSS satellite geometry and attitude models. *Adv. Space Res.* **2015**, *56*, 1015–1029. [CrossRef]
16. Bar-Sever, Y. *Improvement to the GPS Attitude Control Subsystem Enables Predictable Attitude During Eclipse Seasons*; IGS Central Bureau, Jet Propulsion Laboratory: Pasadena, CA, USA, 1994; IGSMAIL-0591.
17. Bar-Sever, Y. Performance Evaluation of the GPS Yaw Bias Implementation. In Proceedings of the 8th International Technical Meetings of the Satellite Division of the Institute of Navigation, Palm Springs, CA, USA, 12–15 September 1995; pp. 599–611.
18. Bar-Sever, Y.; Information Regarding Block IIR Modeling. IGSMAIL-1653. 1997. Available online: http://igscb.jpl.nasa.gov/mail/igsmail/1997/msg00151.html (accessed on 24 June 2021).
19. Dilssner, F. GPS IIF-1 satellite, antenna phase center and attitude modeling. *Inside GNSS* **2010**, *5*, 59–64.
20. Dilssner, F.; Springer, T.; Enderle, W. GPS IIF yaw attitude control during eclipse season. In Proceedings of the AGU Fall Meeting, San Francisco, CA, USA, 5–9 December 2011. Available online: http://acc.igs.org/orbits/yaw-IIF_ESOC_agu11.pdf (accessed on 24 June 2021).

21. Steigenberger, P.; Thoelert, S.; Montenbruck, O. GPS III Vespucci: Results of half a year in orbit. *Adv. Space Res.* **2020**, *66*, 2773–2785. [CrossRef]
22. Lou, Y.; Liu, Y.; Shi, C.; Yao, X.; Zheng, F. Precise orbit determination of BeiDou constellation based on BETS and MGEX network. *Sci. Rep.* **2014**, *4*, 4692. [CrossRef] [PubMed]
23. Dai, X.; Ge, M.; Lou, Y.; Shi, C.; Schuh, H. Estimating the yaw-attitude of BDS IGSO and MEO satellites. *J. Geod.* **2015**, *89*, 1005–1018. [CrossRef]
24. Xia, F.; Ye, S.; Chen, D.; Jiang, N. Observation of BDS-2 IGSO/MEOs yaw-attitude behavior during eclipse seasons. *GPS Solut.* **2019**, *23*, 3. [CrossRef]
25. Lin, X.; Lin, B.; Liu, Y.; Xiong, S.; Bai, T. Satellite Geometry and Attitude Mode of BeiDou-3 MEO satellites Developed by SECM. In Proceedings of the 31th International Technical Meeting of the Satellite Division of the Institute of Navigation (ION GNSS+ 2018), Miami, FL, USA, 24–28 September 2018; pp. 1268–1289.
26. Wang, C.; Guo, J.; Zhao, Q.; Liu, J. Yaw attitude modeling for BeiDou I06 and BeiDou-3 satellites. *GPS Solut.* **2018**, *22*, 117. [CrossRef]
27. GSA. Galileo Satellite Metadata. 2021. Available online: https//www.gsc-europa.eu/support-to-developers/galileo-satellite-metadata (accessed on 24 June 2021).
28. Banville, S.; Geng, J.; Loyer, S.; Schaer, S.; Springer, T.; Strasser, S. On the interoperability of IGS products for precise point positioning with ambiguity resolution. *J. Geod.* **2020**, *94*, 10. [CrossRef]
29. Loyer, S.; Banville, S.; Perosanz, F.; Mercier, F. Disseminating GNSS satellite attitude for improved clock correction consistency. In Proceedings of the 2017 IGS Workshop, Paris, France, 3–7 July 2017. Available online: https://www.researchgate.net/publication/318542441_Disseminating_GNSS_attitude_for_improved_clock_correction_consistency (accessed on 24 June 2021).
30. Geng, J.; Yang, S.; Guo, J. Assessing IGS GPS/Galileo/BDS-2/BDS-3 phase bias products with PRIDE PPP-AR. *Satell. Navig.* **2021**, *2*, 17. [CrossRef]
31. Kouba, J.; Héroux, P. Precise point positioning using IGS orbit and clock products. *GPS Solut.* **2001**, *5*, 12–28. [CrossRef]
32. Johnston, G.; Riddell, A.; Hausler, G. The International GNSS Service. In *Springer Handbook of Global Navigation Satellite Systems*; Springer International Publishing: Berlin/Heidelberg, Germany, 2017; pp. 967–982.
33. Dong, D.; Bock, Y. Global positioning system network analysis with phase ambiguity resolution applied to crustal deformation studies in California. *J. Geophys. Res. Solid Earth* **1989**, *94*, 3949–3966. [CrossRef]
34. Petit, G.; Luzum, B. *IERS Conventions 2010*; IERS Tech. Note 36; Verlag des Bundesamts für Kartographie und Geodäsie: Frankfurt am Main, Germany, 2010. Available online: https://www.iers.org/IERS/EN/Publications/TechnicalNotes/tn36.html (accessed on 24 June 2021).
35. Wanninger, L.; Beer, S. BeiDou satellite-induced code pseudorange variations: Diagnosis and therapy. *GPS Solut.* **2014**, *19*, 639–648. [CrossRef]
36. Wu, J.T.; Wu, S.C.; Hajj, G.A.; Bertiger, W.I.; Lichten, S.M. Effects of antenna orientation on GPS carrier phase. *Manuscr. Geod.* **1993**, *18*, 91–98.